IEEE Control Systems Letters paper presented at
2023 62nd IEEE Conference on Decision and Control (CDC)
December 13-15, 2023. Marina Bay Sands, Singapore

Multivariable Disturbance Observer-Based Finite-Time Sliding Mode Attitude Control for Fixed-Wing UAVs under Matched and Mismatched Disturbances

Ngo Phong Nguyen Hyondong Oh Jun Moon Yoonsoo Kim

Abstract— **In this letter, we propose a multivariable disturbance observer-based finite-time sliding mode attitude control (MDOB-FT-SM-AC) for fixed-wing UAVs in the presence of both matched and mismatched disturbances. Compared with existing sliding mode attitude controllers, the significant improvements of the proposed MDOB-FT-SM-AC are the multivariable control structure, strong robustness, and high precision performance with continuous control input signal. In the proposed MDOB-FT-SM-AC, we first develop multivariable finite-time disturbance observers such that the precise estimation of both matched and mismatched disturbances is ensured. Next, a nonsingular terminal sliding manifold is designed such that the fixed-wing UAV is driven to track its desired attitude command in finite time. We finally present a multivariable super-twisting reaching law such that the finite-time convergence of the sliding variable and its derivative to zero is guaranteed. Attentive finite-time convergence analysis is derived based on the Lyapunov and homogeneity theories. Simulation results are given to illustrate the superiority of the proposed MDOB-FT-SM-AC.**

I. INTRODUCTION

In recent years, unmanned aerial vehicles (UAVs) have received an increasing interest in both control algorithm developments and practical applications [1]. Among various UAV configurations, the fixed-wing UAV has acquired a considerable attention due to its attractive properties such as simple structure, low design cost, long flight range, and high airspeed [1]. Currently, the applications of fixed-wing UAVs can be found in different fields including agriculture mapping, environmental monitoring, and target localization. Under most of these missions, the attitude control is crucial to safe and successful operations. Note that the rotational motions of fixed-wing UAVs are thoroughly influenced by several types of internal and external disturbances (e.g., model perturbations, wind conditions) [1]. Thus, it is essential to design the robust algorithm for the attitude control of fixed-wing UAVs under such disturbed environments.

Over the years, numerous robust solutions were developed for attitude control of fixed-wing UAVs. Among them, the sliding mode control (SMC) in [2]–[8] offers the good robustness (i.e., insensitivity feature) against different kinds of disturbances. Although the effectiveness of the aforementioned SMC for fixed-wing UAVs had been examined in both practical and theoretical aspects, there are still three major technical challenges that require further investigation:

(i) In [2]–[8], the multiple single-channel attitude control laws were designed based on the single-variable sliding mode reaching law. In view of the design perspective, compared with the single-variable scheme, the multivariable scheme is more preferable. In fact, as shown in [1], the fixed-wing UAV attitude dynamics is strongly nonlinear and coupled. Therefore, the multivariable technique might be more appropriate for the fixed-wing UAV because it does not require any decoupling operations during the control design and/or convergence analysis. In view of the implementation perspective, compared with the single-variable scheme, the multivariable scheme is much simpler. In fact, under the same mission, the number of parameters of the multivariable approach is considerably smaller than that of the single-variable one. This implies that the multivariable control scheme is easy to implement;

(ii) The sliding mode attitude controllers in [2]–[8] were developed without the consideration of the influences of mismatched disturbances on the fixed-wing system. As regards of [9], we note that mismatched disturbances refer to disturbances that appear in the different channel with the control input. Meanwhile, matched disturbances mean that disturbances remain in the same channel with the control input. On the one hand, as shown in [1], under several missions, the fixed-wing UAV has to operate in a highly disturbed environment that includes different types of internal and external disturbances (e.g., model perturbations, wind conditions). Note that some of these disturbances (i.e., mismatched disturbances) might directly affect the states rather than through the control input channels. On the other hand, the SMC is insensitive to matched disturbances but sensitive to mismatched disturbances.

This work was supported in part by the Basic Science Research Program through the National Research Foundation (NRF) of Korea Grant funded by the Ministry of Education under Grant 2020R1A6A1A03040570; in part by the NRF of Korea Grant funded by the Ministry of Science and ICT under Grant 2017R1A5A1015311 and Grant 2023R1A2C2003130; and in part by the Institute of Information and Communication Technology Planning and Evaluation (ITTP) Grant funded by the Korea Government (MSIT) under Grant 2020-0-01373. (*Corresponding authors: Hyondong Oh; Jun Moon.*)

Ngo Phong Nguyen and Hyondong Oh are with the Department of Mechanical Engineering, Ulsan National Institute of Science and Technology, Ulsan 44919, South Korea (e-mail: ngophong@unist.ac.kr;h.oh@unist.ac.kr).

Jun Moon is with the Department of Electrical Engineering, Hanyang University, Seoul 04763, South Korea (e-mail: junmoon@hanyang.ac.kr).

Yoonsoo Kim is with Graduate School of Mechanical and Aerospace Engineering, Gyeongsang National University, Jinju 52828, South Korea (e-mail: yoonsoo@gnu.ac.kr).

In other words, in the presence of mismatched disturbances, the sliding mode attitude controllers in [2]–[8] might not ensure the desirable flight performance; and

(iii) The attitude controllers in [2]–[6] only guaranteed the asymptotic stability of the closed-loop system and the attitude controllers in [2], [4]–[6], [8] induced the serious chattering phenomenon owing to the utilization of the discontinuous control component. The asymptotic stability is not preferable as the attitude tracking error only converges to zero when time goes to infinity. The chattering phenomenon is also undesirable for implementation as it might damage the system actuators and degrade the performance of the system.

We here address all aforementioned challenges by proposing the MDOB-FT-SM-AC. We now state the contributions of this work in both practical and theoretical aspects.

Practical contributions: (i) The proposed MDOB-FT-SM-AC generalizes the single-variable SMC structure for the fixed-wing UAV to the case of multivariable structure. Under the proposed MDOB-FT-SM-AC, the control design and convergence analysis are performed without any decoupling operations. This generalization is of important as the fixed-wing UAV attitude dynamics is strongly coupled. Also, compared with the single-variable structure, this multivariable generalization introduces a simpler solution for implementation as the number of control parameters is significantly reduced; (ii) The proposed MDOB-FT-SM-AC ensures the strong robustness of the overall closed-loop system against disturbances. In particular, under the MDOB-FT-SM-AC, the overall closed-loop system is insensitive to both matched and mismatched disturbances. This feature is of important since under some control missions, the fixed-wing system has to perform safe and successful operations in a highly disturbed environment; and (iii) The proposed MDOB-FT-SM-AC generates the continuous control input signal. This feature is of important as the system actuators are protected and smooth movement of the fixed-wing UAV is achieved.

Theoretical contributions: (i) The proposed MDOB-FT-SM-AC belongs to a class of multivariable finite time control. This feature is of important as the proposed MDOB-FT-SM-AC ensures that the fixed-wing UAV is driven to track its desired command in finite time; and (ii) Rigorous convergence finite-time analysis of the closed-loop system is given based on the Lyapunov and homogeneity theories.[1]

Notations: For a vector $\mathbf{x} \in \mathbb{R}^n$, $\|\mathbf{x}\|$ is the Euclidean norm of $\mathbf{x}$. For a positive definite matrix $\mathbf{P} \in \mathbb{R}^{n\times n}$, $\lambda_{\max}\{\mathbf{P}\}$ and $\lambda_{\min}\{\mathbf{P}\}$ denote the largest and smallest eigenvalues of $\mathbf{P}$.

II. PROBLEM FORMULATION

In view of [1]–[8], the attitude dynamics of the disturbed fixed-wing UAV can be described as follows:

$$\dot{\boldsymbol{\Theta}} = \mathbf{R}\boldsymbol{\omega} + \mathbf{d}_1,\ \mathbf{I}\dot{\boldsymbol{\omega}} = -\boldsymbol{\omega} \times (\mathbf{I}\boldsymbol{\omega}) + \mathbf{M} + \mathbf{d}_2, \quad (1)$$

where $\boldsymbol{\Theta} = [\phi \quad \theta \quad \psi]^\top \in \mathbb{R}^3$ denotes the Euler angle vector, $\boldsymbol{\omega} = [p \quad q \quad r]^\top \in \mathbb{R}^3$ represents the angular rate vector, $\mathbf{M} \in \mathbb{R}^3$ is the control input vector, $\mathbf{d}_1 \in \mathbb{R}^3$ and $\mathbf{d}_2 \in \mathbb{R}^3$ stand for the mismatched and matched disturbance vectors, respectively, and $\mathbf{R}, \mathbf{I} \in \mathbb{R}^{3\times 3}$ denote the transformation and inertia matrices, respectively, that are defined as

$$\mathbf{R} = \begin{bmatrix} 1 & \sin(\phi)\tan(\theta) & \cos(\phi)\tan(\theta) \\ 0 & \cos(\phi) & -\sin(\phi) \\ 0 & \sin(\phi)\sec(\theta) & \cos(\phi)\sec(\theta) \end{bmatrix}$$
$$\mathbf{I} = \begin{bmatrix} I_x & -I_{xy} & -I_{xz} \\ -I_{xy} & I_y & -I_{yz} \\ -I_{xz} & -I_{yz} & I_z \end{bmatrix}, \quad (2)$$

with $I_x, I_y, I_z, I_{xy}, I_{xz}$, and I_{yz} are rotational inertias. Here, $\boldsymbol{\Theta}$ and $\boldsymbol{\omega}$ are assumed to be available for the control design.

Assumption 1: For system (1), the Euler angles (i.e., ϕ, θ, and ψ) satisfy $\phi, \theta \in (-\pi/2, \pi/2)$ and $\psi \in (-\pi, \pi]$.

Assumption 2: The time-varying mismatched and matched disturbances in (1) fulfill the following circumstances: (i) $\mathbf{d}_1$ is second-order differentiable and $\|\mathbf{d}_1\|, \|\dot{\mathbf{d}}_1\|, \|\ddot{\mathbf{d}}_1\| \leq L_1$; and (ii) $\mathbf{d}_2$ is differentiable and $\|\mathbf{d}_2\|, \|\dot{\mathbf{d}}_2\| \leq L_2$, where L_1 and L_2 are known positive constants.

Remark 1: Taking into consideration of mechanical constraints, Assumption 1 is mild and sensible for the (practical) fixed-wing UAV. Also, Assumption 2 is weak and reasonable as disturbances acting on the fixed-wing UAV generally have finite energy with bounded changing rates (see also [1]–[8]).

Remark 2: Compared with the corresponding rotational equations of the fixed-wing UAV in [2]–[8], the considered dynamics in (1) are more reasonable for a practical system. In fact, the mismatched disturbance $\mathbf{d}_1$ is used to describe the influences of internal perturbations due to model simplification, actuator failure, and measurement bias as well as the effects of discretization in practical implementation. Meanwhile, the matched disturbance $\mathbf{d}_2$ is included to illustrate the effects of wind conditions and model uncertainties.

Control objective: For the system (1) with Assumption 1 and 2, we design a new attitude control structure, without any decoupling operations to the original rotational dynamics, which ensures the fixed-wing UAV to converge to its desired command in finite time under continuous control signal.

III. MAIN RESULTS

A. Tracking error dynamics

We first introduce the auxiliary variable as $\overline{\boldsymbol{\omega}} = \mathbf{R}\boldsymbol{\omega}$. The time derivative of $\overline{\boldsymbol{\omega}}$ along the dynamics in (1) is as

$$\dot{\overline{\boldsymbol{\omega}}} = \dot{\mathbf{R}}\boldsymbol{\omega} - \mathbf{R}\mathbf{I}^{-1}\big[\boldsymbol{\omega} \times (\mathbf{I}\boldsymbol{\omega})\big] + \mathbf{R}\mathbf{I}^{-1}\mathbf{M} + \mathbf{R}\mathbf{I}^{-1}\mathbf{d}_2. \quad (3)$$

From (1) and (3), the following equivalent dynamics is given:

$$\dot{\boldsymbol{\Theta}} = \overline{\boldsymbol{\omega}} + \mathbf{d}_1,\ \dot{\overline{\boldsymbol{\omega}}} = \mathbf{F} + \mathbf{R}\mathbf{I}^{-1}\mathbf{M} + \overline{\mathbf{d}}_2, \quad (4)$$

where $\mathbf{F}$ and $\overline{\mathbf{d}}_2$ are described as follows:

$$\mathbf{F} = -\mathbf{R}\mathbf{I}^{-1}\big\{(\mathbf{R}^{-1}\overline{\boldsymbol{\omega}}) \times \big[\mathbf{I}(\mathbf{R}^{-1}\overline{\boldsymbol{\omega}})\big]\big\}$$
$$\overline{\mathbf{d}}_2 = \dot{\mathbf{R}}(\mathbf{R}^{-1}\overline{\boldsymbol{\omega}}) + \mathbf{R}\mathbf{I}^{-1}\mathbf{d}_2. \quad (5)$$

[1]Note that an additional theoretical contribution of this work can be found in the discussions provided in Remarks 5 and 6.

Now, for the equivalent system in (4), we define the following tracking errors: $\mathbf{e}_1 = \boldsymbol{\Theta} - \boldsymbol{\Theta}_{\rm ref}, \mathbf{e}_2 = \overline{\boldsymbol{\omega}} - \dot{\boldsymbol{\Theta}}_{\rm ref}$, where $\mathbf{e}_1$ denotes the attitude tracking error vector, $\mathbf{e}_2$ represents auxiliary (angular speed) tracking error vector, and $\boldsymbol{\Theta}_{\rm ref}$ and $\dot{\boldsymbol{\Theta}}_{\rm ref}$ represent the desired command vector and its corresponding derivative. Here, we suppose that $\boldsymbol{\Theta}_{\rm ref}$ and its (consecutive) derivatives are bounded. Then, by taking the derivative of $\mathbf{e}_1$ and $\mathbf{e}_2$ along the system dynamics in (4), we acquire the following (attitude) tracking error dynamics:

$$\dot{\mathbf{e}}_1 = \mathbf{e}_2 + \mathbf{d}_1,\ \dot{\mathbf{e}}_2 = \mathbf{F} - \ddot{\boldsymbol{\Theta}}_{\rm ref} + \mathbf{R}\mathbf{I}^{-1}\mathbf{M} + \overline{\mathbf{d}}_2. \quad (6)$$

Remark 3: (i) In view of Eq. (2) with Assumption 1, the matrix $\mathbf{R}$ is invertible. Besides, the matrix $\mathbf{I}$ is generally invertible with the proper mechanical design. Hence, the dynamics in (6) are well-defined; and

(ii) In view of Assumptions 1 and 2 with examination of mechanical constraints of the (practical) fixed-wing UAV, it is reasonable to consider that the matched disturbances $\overline{\mathbf{d}}_2$ in (6) is differentiable and $\|\overline{\mathbf{d}}_2\|, \|\dot{\overline{\mathbf{d}}}_2\| \leq \overline{L}_2$, where $\overline{L}_2$ is known positive constant.

B. Control design

1) Multivariable finite-time disturbance observers design: We introduce the following multivariable finite-time mismatched disturbance observer:

$$\begin{aligned}
&\dot{\mathbf{z}}_{01} = \mathbf{v}_{01} + \mathbf{e}_2, \dot{\mathbf{z}}_{11} = \mathbf{v}_{11}, \dot{\mathbf{z}}_{21} = \mathbf{v}_{21}\\
&\mathbf{v}_{01} = \lambda_{01}\|\mathbf{e}_1 - \mathbf{z}_{01}\|^{2/3}\frac{(\mathbf{e}_1 - \mathbf{z}_{01})}{\|\mathbf{e}_1 - \mathbf{z}_{01}\|} + \mathbf{z}_{11}\\
&\mathbf{v}_{11} = \lambda_{11}\|\mathbf{e}_1 - \mathbf{z}_{01}\|^{1/3}\frac{(\mathbf{e}_1 - \mathbf{z}_{01})}{\|\mathbf{e}_1 - \mathbf{z}_{01}\|} + \mathbf{z}_{21}\\
&\mathbf{v}_{21} = \lambda_{21}\frac{(\mathbf{e}_1 - \mathbf{z}_{01})}{\|\mathbf{e}_1 - \mathbf{z}_{01}\|}, \qquad (7)
\end{aligned}$$

and multivariable finite-time matched disturbance observer:

$$\begin{aligned}
&\dot{\mathbf{z}}_{02} = \mathbf{v}_{02} + \mathbf{F} - \ddot{\boldsymbol{\Theta}}_{\rm ref} + \mathbf{R}\mathbf{I}^{-1}\mathbf{M}, \dot{\mathbf{z}}_{12} = \mathbf{v}_{12}\\
&\mathbf{v}_{02} = \lambda_{02}\|\mathbf{e}_2 - \mathbf{z}_{02}\|^{1/2}\frac{(\mathbf{e}_2 - \mathbf{z}_{02})}{\|\mathbf{e}_2 - \mathbf{z}_{02}\|} + \mathbf{z}_{12}\\
&\mathbf{v}_{12} = \lambda_{12}\frac{(\mathbf{e}_2 - \mathbf{z}_{02})}{\|\mathbf{e}_2 - \mathbf{z}_{02}\|}, \qquad (8)
\end{aligned}$$

where $\lambda_{01}, \lambda_{11}, \lambda_{21}, \lambda_{02}$, and $\lambda_{12} > 0$ are observer coefficients. Note that these coefficients are selected appropriately based on the bounds of $\ddot{\mathbf{d}}_1$ and $\dot{\overline{\mathbf{d}}}_2$, which are defined in Assumption 2 and Remark 3 (see [10] for relevant discussions). For the disturbance observer (7), $\mathbf{z}_{01}, \mathbf{z}_{11}$, and $\mathbf{z}_{21}$ denote the estimates of $\mathbf{e}_1, \mathbf{d}_1$, and $\dot{\mathbf{d}}_1$, respectively. For the disturbance observer (8), $\mathbf{z}_{02}$ and $\mathbf{z}_{12}$ represent the estimates of $\mathbf{e}_2$ and $\overline{\mathbf{d}}_2$, respectively.

2) MDOB-FT-SM-AC design: The nonsingular terminal sliding manifold is now developed with the sliding variable defined as

$$\mathbf{s} = \mathbf{e}_2 + \mathbf{z}_{11} + \int_0^t \left[k_1\|\mathbf{e}_1\|^{r_1}\frac{\mathbf{e}_1}{\|\mathbf{e}_1\|} + k_2\|\mathbf{e}_2 + \mathbf{z}_{11}\|^{r_2}\frac{(\mathbf{e}_2 + \mathbf{z}_{11})}{\|\mathbf{e}_2 + \mathbf{z}_{11}\|}\right]\mathrm{d}\tau, \quad (9)$$

where k_1 and k_2 are positive constants, $r_1 = r_2/(2-r_2)$ with $r_2 \in (0,1)$, and $\mathbf{z}_{11}$ is given from (7). Next, by utilizing the multivariable super-twisting reaching law, the MDOB-FT-SM-AC is designed as

$$\mathbf{M} = \mathbf{I}\mathbf{R}^{-1}\Big\{ -\mathbf{F} + \ddot{\boldsymbol{\Theta}}_{\rm ref} - \mathbf{v}_{11} - \mathbf{z}_{12} - \Big[k_1\|\mathbf{e}_1\|^{r_1}\frac{\mathbf{e}_1}{\|\mathbf{e}_1\|} + k_2\|\mathbf{e}_2 + \mathbf{z}_{11}\|^{r_2}\frac{(\mathbf{e}_2 + \mathbf{z}_{11})}{\|\mathbf{e}_2 + \mathbf{z}_{11}\|}\Big] + \mathbf{u}_r\Big\}, \quad (10)$$

where $\mathbf{v}_{11}$ is given from (7), $\mathbf{z}_{12}$ is provided in (8), and the multivariable super-twisting reaching law $\mathbf{u}_r$ is defined as

$$\mathbf{u}_r = -\beta_1\|\mathbf{s}\|^{1/2}\frac{\mathbf{s}}{\|\mathbf{s}\|} - \beta_2\mathbf{s} + \mathbf{z},\ \dot{\mathbf{z}} = -\beta_3\frac{\mathbf{s}}{\|\mathbf{s}\|} - \beta_4\mathbf{s}, \quad (11)$$

where $\beta_1, \beta_2, \beta_3$ and β_4 are positive constants, which satisfy the following condition: $4\beta_3\beta_4 > (8\beta_3 + 9\beta_1^2)\beta_2^2$. Note that, as shown in Remark 3, the matrix $\mathbf{R}$ is invertible, and thus, the MDOB-FT-SM-AC in (10) is well-defined. Besides, for implementation, $\mathbf{R}$ and $\mathbf{F}$ can be calculated at each timestep in view of their definitions in (2) and (5), respectively.

C. Convergence analysis

Theorem 1: For the (attitude) tracking error dynamics in (6) with Assumptions 1 and 2, the proposed MDOB-FT-SM-AC renders the following properties: (i) the multivariable disturbance observers in (7) and (8) ensure the finite-time accurate estimation of disturbances and its derivative. In other words, under the disturbance observers in (7) and (8), $\mathbf{z}_{01} = \mathbf{e}_1, \mathbf{z}_{11} = \mathbf{d}_1, \mathbf{z}_{21} = \dot{\mathbf{d}}_1$ and $\mathbf{z}_{02} = \mathbf{e}_2, \mathbf{z}_{12} = \overline{\mathbf{d}}_2$ are established in finite time, respectively; (ii) the multivariable super-twisting reaching law $\mathbf{u}_r$ in (11) guarantees that the sliding variable $\mathbf{s}$ and its derivative $\dot{\mathbf{s}}$ converge to zero in finite time during the reaching phase; and (iii) the nonsingular terminal sliding manifold in (9) ensures that the attitude tracking error $\mathbf{e}_1$ converges to zero during the sliding phase.

Proof. The proof of Theorem 1 is divided into three parts. We first show the convergence of the disturbance observers in (7) and (8). Then, in the second and third parts, attentive examination are provided to show the finite-time convergence feature of sliding variable $\mathbf{s}$ and attitude tracking error $\mathbf{e}_1$ during the reaching and sliding phases, respectively. We now begin with the first part of the proof.

Part 1: The estimation error variables of the disturbance observer in (7) are first introduced as $\boldsymbol{\sigma}_{01} = \mathbf{e}_1 - \mathbf{z}_{01}, \boldsymbol{\sigma}_{11} = \mathbf{d}_1 - \mathbf{z}_{11}, \boldsymbol{\sigma}_{21} = \dot{\mathbf{d}}_1 - \mathbf{z}_{21}$. Then, from (6) and (7), the estimation error dynamics of the disturbance observer in (7) are given as

$$\begin{aligned}
&\dot{\boldsymbol{\sigma}}_{01} = -\lambda_{01}\|\boldsymbol{\sigma}_{01}\|^{2/3}\frac{\boldsymbol{\sigma}_{01}}{\|\boldsymbol{\sigma}_{01}\|} + \boldsymbol{\sigma}_{11}\\
&\dot{\boldsymbol{\sigma}}_{11} = -\lambda_{11}\|\boldsymbol{\sigma}_{01}\|^{1/3}\frac{\boldsymbol{\sigma}_{01}}{\|\boldsymbol{\sigma}_{01}\|} + \boldsymbol{\sigma}_{21}\\
&\dot{\boldsymbol{\sigma}}_{21} = -\lambda_{21}\frac{\boldsymbol{\sigma}_{01}}{\|\boldsymbol{\sigma}_{01}\|} + \ddot{\mathbf{d}}_1. \qquad (12)
\end{aligned}$$

We now introduce the estimation error variables of the disturbance observer in (8) as $\boldsymbol{\sigma}_{02} = \mathbf{e}_2 - \mathbf{z}_{02}, \boldsymbol{\sigma}_{12} = \overline{\mathbf{d}}_2 - \mathbf{z}_{12}$.

Then, from (6) and (8), the estimation error dynamics of the disturbance observer in (8) are expressed as

$$\dot{\boldsymbol{\sigma}}_{02} = -\lambda_{02}\|\boldsymbol{\sigma}_{02}\|^{1/2}\frac{\boldsymbol{\sigma}_{02}}{\|\boldsymbol{\sigma}_{02}\|} + \boldsymbol{\sigma}_{12}$$
$$\dot{\boldsymbol{\sigma}}_{12} = -\lambda_{12}\frac{\boldsymbol{\sigma}_{02}}{\|\boldsymbol{\sigma}_{02}\|} + \dot{\overline{\mathbf{d}}}_2. \tag{13}$$

In view of [10], [11], the dynamics in (12) and (13) are finite-time stable with proper observer coefficients. In other words, $\mathbf{z}_{01} = \mathbf{e}_1, \mathbf{z}_{11} = \mathbf{d}_1, \mathbf{z}_{21} = \dot{\mathbf{d}}_1$ and $\mathbf{z}_{02} = \mathbf{e}_2, \mathbf{z}_{12} = \overline{\mathbf{d}}_2$ are exhibited in some finite time T_1 and T_2, respectively. This completes the first part of the proof.

Part 2: First, the time derivative of $\mathbf{s}$ in (9) along the tracking error dynamics in (6) can be obtained as

$$\dot{\mathbf{s}} = \mathbf{F} - \ddot{\boldsymbol{\Theta}}_{\mathrm{ref}} + \mathbf{R}\mathbf{I}^{-1}\mathbf{M} + \overline{\mathbf{d}}_2 + \dot{\mathbf{z}}_{11} + k_1\|\mathbf{e}_1\|^{r_1}\frac{\mathbf{e}_1}{\|\mathbf{e}_1\|} + k_2\|\mathbf{e}_2 + \mathbf{z}_{11}\|^{r_2}\frac{(\mathbf{e}_2 + \mathbf{z}_{11})}{\|\mathbf{e}_2 + \mathbf{z}_{11}\|}. \tag{14}$$

Then, by substituting the proposed MDOB-FT-SM-AC in (10) and (11) into (14), the sliding variable dynamics are given as follows:

$$\dot{\mathbf{s}} = -\beta_1\|\mathbf{s}\|^{1/2}\frac{\mathbf{s}}{\|\mathbf{s}\|} - \beta_2\mathbf{s} + \mathbf{z} + \boldsymbol{\sigma}_{12},\ \dot{\mathbf{z}} = -\beta_3\frac{\mathbf{s}}{\|\mathbf{s}\|} - \beta_4\mathbf{s}. \tag{15}$$

Note that as represented in (15), the sliding variable dynamics are suffered from the estimation error dynamics (13). Hence, before investigating the convergence property of the dynamics in (15), it is crucial to show that the estimation error dynamics in (13) do not drive the sliding variable dynamics in (15) to infinity in a finite-time interval. In that context, we consider the following positive definite function:

$$V_1 = \frac{1}{2}\mathbf{s}^\top\mathbf{s} + \frac{1}{2}\mathbf{z}^\top\mathbf{z}. \tag{16}$$

By taking the time derivative of V_1 in (16) along the sliding variable dynamics in (15), we obtain

$$\begin{aligned}\dot{V}_1 &= \mathbf{s}^\top\Big(-\beta_1\|\mathbf{s}\|^{1/2}\frac{\mathbf{s}}{\|\mathbf{s}\|} - \beta_2\mathbf{s} + \mathbf{z} + \boldsymbol{\sigma}_{12}\Big) + \mathbf{z}^\top\Big(-\beta_3\frac{\mathbf{s}}{\|\mathbf{s}\|} - \beta_4\mathbf{s}\Big)\\ &\le -\beta_1\|\mathbf{s}\|^{3/2} - \beta_2\|\mathbf{s}\|^2 + \|\mathbf{s}\|\|\mathbf{z}\| + \|\mathbf{s}\|\|\boldsymbol{\sigma}_{12}\| + \beta_3\|\mathbf{z}\| + \beta_4\|\mathbf{s}\|\|\mathbf{z}\|\\ &\le \|\mathbf{s}\|\|\mathbf{z}\| + \|\mathbf{s}\|\|\boldsymbol{\sigma}_{12}\| + \beta_3\|\mathbf{z}\| + \beta_4\|\mathbf{s}\|\|\mathbf{z}\|\\ &\le (1+\beta_4)\frac{\|\mathbf{s}\|^2 + \|\mathbf{z}\|^2}{2} + \sigma\frac{\|\mathbf{s}\|^2 + 1}{2} + \beta_3\frac{\|\mathbf{z}\|^2 + 1}{2}\\ &\le \overline{K}_1 V_1 + \overline{L}_1,\end{aligned} \tag{17}$$

where σ is a positive constant such that $\|\boldsymbol{\sigma}_{12}\| \le \sigma$ in view of the first part of the proof and $\overline{K}_1 = \beta_3 + \beta_4 + \sigma + 1$ and $\overline{L}_1 = \frac{1}{2}(\beta_3 + \sigma)$ are bounded (positive) constants. Therefore, in view of (17), we can conclude that V_1, and thus, $\mathbf{s}$ and $\mathbf{z}$, remain bounded for a finite-time interval. We now investigate the finite-time convergence feature of the sliding variable dynamics in (15). As shown in the first part of the proof, $\boldsymbol{\sigma}_{12}$ converges to zero in some finite time T_2. Besides, as we discussed above, $\mathbf{s}$ and $\mathbf{z}$ remain bounded for a finite-time interval. In that context, when $t \ge \mathrm{T}_2$, the sliding variable dynamics in (15) are further expressed as

$$\dot{\mathbf{s}} = -\beta_1\frac{\mathbf{s}}{\|\mathbf{s}\|^{1/2}} - \beta_2\mathbf{s} + \mathbf{z},\ \dot{\mathbf{z}} = -\beta_3\frac{\mathbf{s}}{\|\mathbf{s}\|} - \beta_4\mathbf{s}. \tag{18}$$

For system (18), by utilizing the ideas in [12], we consider the following Lyapunov function candidate:

$$V_2 = \Big(2\beta_3 + \frac{\beta_1^2}{2}\Big)\|\mathbf{s}\| + \Big(\beta_4 + \frac{\beta_2^2}{2}\Big)\mathbf{s}^\top\mathbf{s} + \mathbf{z}^\top\mathbf{z} + \beta_1\beta_2\frac{\mathbf{s}^\top\mathbf{s}}{\|\mathbf{s}\|^{1/2}} - \beta_2\mathbf{s}^\top\mathbf{z} - \beta_1\frac{\mathbf{z}^\top\mathbf{s}}{\|\mathbf{s}\|^{1/2}}. \tag{19}$$

Then, by taking the time derivative of V_2, we obtain

$$\begin{aligned}\dot{V}_2 = &\Big(2\beta_3 + \frac{\beta_1^2}{2}\Big)\frac{\mathbf{s}^\top\dot{\mathbf{s}}}{\|\mathbf{s}\|} + \big(2\beta_4 + \beta_2^2\big)\mathbf{s}^\top\dot{\mathbf{s}} + 2\mathbf{z}^\top\dot{\mathbf{z}} + \frac{3}{2}\beta_1\beta_2\frac{\mathbf{s}^\top\dot{\mathbf{s}}}{\|\mathbf{s}\|^{1/2}} - \beta_2\big(\dot{\mathbf{s}}^\top\mathbf{z} + \mathbf{s}^\top\dot{\mathbf{z}}\big)\\ &- \beta_1\Big(-\frac{1}{2}\frac{(\mathbf{s}^\top\dot{\mathbf{s}})(\mathbf{z}^\top\mathbf{s})}{\|\mathbf{s}\|^{5/2}} + \frac{\dot{\mathbf{z}}^\top\mathbf{s} + \mathbf{z}^\top\dot{\mathbf{s}}}{\|\mathbf{s}\|^{1/2}}\Big).\end{aligned}$$

From the sliding variable dynamics in (18), we can verify

$$\begin{aligned}\dot{V}_2 \le &-\Big(\beta_1\beta_3 + \frac{\beta_1^3}{2}\Big)\|\mathbf{s}\|^{1/2} - \big(\beta_2\beta_3 + 2\beta_1^2\beta_2\big)\|\mathbf{s}\|\\ &- \Big(\beta_1\beta_4 + \frac{5}{2}\beta_1\beta_2^2\Big)\|\mathbf{s}\|^{3/2} - \big(\beta_2\beta_4 + \beta_2^3\big)\|\mathbf{s}\|^2\\ &+ \beta_1^2\|\mathbf{z}\| + 2\beta_2^2\|\mathbf{s}\|\|\mathbf{z}\| + 3\beta_1\beta_2\|\mathbf{s}\|^{1/2}\|\mathbf{z}\|\\ &- \beta_2\|\mathbf{z}\|^2 - \frac{\beta_1}{2}\frac{\|\mathbf{z}\|^2}{\|\mathbf{s}\|^{1/2}}.\end{aligned} \tag{20}$$

Next, we define the state vector: $\mathbf{x} = \begin{bmatrix}\|\mathbf{s}\|^{1/2} & \|\mathbf{s}\| & \|\mathbf{z}\|\end{bmatrix}^\top$. Then, from (20), we obtain

$$\dot{V}_2 \le -\frac{1}{\|\mathbf{s}\|^{1/2}}\mathbf{x}^\top\boldsymbol{\Omega}_{\mathbf{1}}\mathbf{x} - \mathbf{x}^\top\boldsymbol{\Omega}_{\mathbf{2}}\mathbf{x}, \tag{21}$$

where the matrices $\boldsymbol{\Omega}_{\mathbf{1}}$ and $\boldsymbol{\Omega}_{\mathbf{2}}$ are defined as

$$\boldsymbol{\Omega}_{\mathbf{1}} = \begin{bmatrix}\frac{1}{2}\beta_1^3 + \beta_1\beta_3 & 0 & -\frac{1}{2}\beta_1^2\\ 0 & \beta_1\beta_4 + \frac{5}{2}\beta_1\beta_2^2 & -\frac{3}{2}\beta_1\beta_2\\ -\frac{1}{2}\beta_1^2 & -\frac{3}{2}\beta_1\beta_2 & \frac{1}{2}\beta_1\end{bmatrix}$$
$$\boldsymbol{\Omega}_{\mathbf{2}} = \begin{bmatrix}\beta_2\beta_3 + 2\beta_1^2\beta_2 & 0 & 0\\ 0 & \beta_2\beta_4 + \beta_2^3 & -\beta_2^2\\ 0 & -\beta_2^2 & \beta_2\end{bmatrix}.$$

We can validate that $\boldsymbol{\Omega}_{\mathbf{1}} > 0$ and $\boldsymbol{\Omega}_{\mathbf{2}} > 0$ if the following conditions are satisfied:

$$4\beta_3\beta_4 > (8\beta_3 + 9\beta_1^2)\beta_2^2,\ \beta_i > 0, i = 1, \ldots, 4.$$

Hence, from (21), we can derive

$$\dot{V}_2 \le -\frac{1}{\|\mathbf{s}\|^{1/2}}\mathbf{x}^\top\boldsymbol{\Omega}_{\mathbf{1}}\mathbf{x} \le -\frac{1}{\|\mathbf{s}\|^{1/2}}\lambda_{\min}(\boldsymbol{\Omega}_{\mathbf{1}})\|\mathbf{x}\|^2, \tag{22}$$

in view of Rayleigh's inequality. Now, by defining the new state vector $\mathbf{X} = \begin{bmatrix}\frac{\mathbf{s}}{\|\mathbf{s}\|^{1/2}} & \mathbf{s} & \mathbf{z}\end{bmatrix}^\top$, it can be validated that $\|\mathbf{X}\| = \|\mathbf{x}\|$. Thus, we can rewrite (22) as follows:

$$\dot{V}_2 \le -\frac{1}{\|\mathbf{s}\|^{1/2}}\lambda_{\min}(\boldsymbol{\Omega}_{\mathbf{1}})\|\mathbf{X}\|^2. \tag{23}$$

We mention that the Lyapunov function V_2 (see (19)) might also be expressed in the quadratic form $V_2 = \mathbf{X}^\top \mathbf{P} \mathbf{X}$ with the proper symmetric positive definite matrix $\mathbf{P}$. Therefore, in view of the Rayleigh's inequality and the fact that $\|\mathbf{s}\|^{1/2} \leq \|\mathbf{X}\| \leq \frac{V_2^{1/2}}{\lambda_{\min}^{1/2}(\mathbf{P})}$, from (23), we have

$$\dot{V}_2 \leq -\frac{\lambda_{\min}^{1/2}(\mathbf{P})\lambda_{\min}(\mathbf{\Omega}_1)}{\lambda_{\max}(\mathbf{P})} V_2^{1/2}. \tag{24}$$

In view of (24), V_2, and thus, $\mathbf{s}$ and $\mathbf{z}$, converge to zero in some finite time T_3. Then, from (18), $\dot{\mathbf{s}}$ also converges to zero as $t \geq \mathrm{T}_3$. This completes the second part of the proof.

Part 3: We first define the new state variables as $\overline{\mathbf{e}}_1 = \mathbf{e}_1$ and $\overline{\mathbf{e}}_2 = \mathbf{e}_2 + \mathbf{z}_{11}$. Then, we can obtain the following equivalent (attitude) tracking error dynamics:

$$\dot{\overline{\mathbf{e}}}_1 = \overline{\mathbf{e}}_2 + \boldsymbol{\sigma}_{11}, \dot{\overline{\mathbf{e}}}_2 = -k_1 \|\overline{\mathbf{e}}_1\|^{r_1} \frac{\overline{\mathbf{e}}_1}{\|\overline{\mathbf{e}}_1\|} - k_2 \|\overline{\mathbf{e}}_2\|^{r_2} \frac{\overline{\mathbf{e}}_2}{\|\overline{\mathbf{e}}_2\|} + \dot{\mathbf{s}}. \tag{25}$$

As shown in (25), the equivalent tracking error dynamics are suffered from the dynamics in both (12) and (15). Hence, before investigating the finite-time convergence feature of $\overline{\mathbf{e}}_1$, it is crucial to ensure that the dynamics in (12) and (15) do not force the equivalent tracking error dynamics in (25) to infinity in finite time. In that context, we consider the following positive definite function [16]:

$$V_3 = \|\overline{\mathbf{e}}_1\| + \|\overline{\mathbf{e}}_2\|. \tag{26}$$

The time derivative of V_3 in (26) along the equivalent tracking error dynamics in (25) is given as

$$\begin{aligned} \dot{V}_3 &= \frac{1}{\|\overline{\mathbf{e}}_1\|} \overline{\mathbf{e}}_1^\top \left(\overline{\mathbf{e}}_2 + \boldsymbol{\sigma}_{11}\right) \\ &\quad + \frac{1}{\|\overline{\mathbf{e}}_2\|} \overline{\mathbf{e}}_2^\top \left(- k_1 \|\overline{\mathbf{e}}_1\|^{r_1} \frac{\overline{\mathbf{e}}_1}{\|\overline{\mathbf{e}}_1\|} - k_2 \|\overline{\mathbf{e}}_2\|^{r_2} \frac{\overline{\mathbf{e}}_2}{\|\overline{\mathbf{e}}_2\|} + \dot{\mathbf{s}} \right) \\ &\leq V_3 + 2\max\{k_1, k_2\} \max\{V_3^{r_1}, V_3^{r_2}\} + \overline{L}, \end{aligned} \tag{27}$$

where $\overline{L}$ is a positive constant such that $\|\boldsymbol{\sigma}_{11}\| + \|\dot{\mathbf{s}}\| \leq \overline{L}$ in view of *Parts 1* and *2*. We consider the following cases:

Case 1: For $V_3 \leq 1$, it is straightforward to conclude that $\|\overline{\mathbf{e}}_1\|$ and $\|\overline{\mathbf{e}}_2\|$ remain bounded in a finite-time interval.

Case 2: For $V_3 > 1$, Eq. (27) can be further expressed as $\dot{V}_3 \leq (1 + 2\max\{k_1, k_2\}) V_3 + \overline{L}$, which implies that V_3, and thus, $\|\overline{\mathbf{e}}_1\|$ and $\|\overline{\mathbf{e}}_2\|$, stay bounded in a finite-time interval.

Hence, from the aforementioned two cases, we can state that for a finite-time interval, $\|\overline{\mathbf{e}}_1\|$ and $\|\overline{\mathbf{e}}_2\|$ stay bounded. Now, as illustrated in the first and second parts of the proof, $\boldsymbol{\sigma}_{11}$ and $\dot{\mathbf{s}}$ converge to zero in some finite time $\mathrm{T}_4 = \max\{\mathrm{T}_1, \mathrm{T}_3\}$. Note also that as we discussed above, $\overline{\mathbf{e}}_1$ and $\overline{\mathbf{e}}_2$ remain bounded for a finite-time interval. In that context, when $t \geq \mathrm{T}_4$, the equivalent tracking error dynamics (25) can be further expressed as

$$\dot{\overline{\mathbf{e}}}_1 = \overline{\mathbf{e}}_2, \dot{\overline{\mathbf{e}}}_2 = -k_1 \|\overline{\mathbf{e}}_1\|^{r_1} \frac{\overline{\mathbf{e}}_1}{\|\overline{\mathbf{e}}_1\|} - k_2 \|\overline{\mathbf{e}}_2\|^{r_2} \frac{\overline{\mathbf{e}}_2}{\|\overline{\mathbf{e}}_2\|}. \tag{28}$$

In view of [13], [14], [16], we introduce the following Lyapunov function candidate:

$$V_4 = \|\overline{\mathbf{e}}_1\|^{r_1+1} + \frac{r_1+1}{2k_1} \|\overline{\mathbf{e}}_2\|^2. \tag{29}$$

Then, by taking the derivative of V_4 in (29) along the equivalent tracking error dynamics in (28), we have

$$\begin{aligned} \dot{V}_4 &= (r_1+1)\|\overline{\mathbf{e}}_1\|^{r_1} \frac{\overline{\mathbf{e}}_1^\top \dot{\overline{\mathbf{e}}}_1}{\|\overline{\mathbf{e}}_1\|} + \frac{r_1+1}{k_1} \|\overline{\mathbf{e}}_2\| \frac{\overline{\mathbf{e}}_2^\top \dot{\overline{\mathbf{e}}}_2}{\|\overline{\mathbf{e}}_2\|} \\ &= -\frac{k_2(r_1+1)}{k_1} \|\overline{\mathbf{e}}_2\|^{r_2+1} \leq 0, \end{aligned}$$

and thus, $\dot{V}_4$ is negative semi-definite. In view of the LaSalle theorem, we can observe that the set $\Lambda = \{\dot{V}_4 = 0\}$ includes of $\overline{\mathbf{e}}_2 = 0$. Besides, we can easily investigate that the only invariant set inside $\overline{\mathbf{e}}_2 = \mathbf{0}$ is $\overline{\mathbf{e}}_1 = \overline{\mathbf{e}}_2 = \mathbf{0}$. Hence, $\overline{\mathbf{e}}_1$ and $\overline{\mathbf{e}}_2$ will converge to zero asymptotically [13]. Now, by considering the vector field (28) and the dilation $\left(\frac{2-r_2}{1-r_2}, \frac{2-r_2}{1-r_2}, \frac{2-r_2}{1-r_2}, \frac{1}{1-r_2}, \frac{1}{1-r_2}, \frac{1}{1-r_2}\right)$, we can observe that the vector field (28) is homogeneous of degree -1. Therefore, in view of [14], the dynamics in (28) is finite-time stable. In other words, the attitude tracking error $\overline{\mathbf{e}}_1$ (i.e., $\mathbf{e}_1$) converges to zero in finite time. We complete the proof. □

Remark 4: This work mainly concentrates on the design of the new attitude control structure for fixed-wing UAVs. The signal measurement and processing are different problems, which are beyond the scope of this paper. Hence, the influences of measurement noises are neglected during the control design and analysis. Meanwhile, the robustness of the closed-loop system under measurement noises is investigated through numerical simulation in Section IV.

Remark 5: The MDOB-FT-SM-AC can generally be applied into the following disturbed multivariable integrator system:

$$\dot{\mathbf{x}}_1 = \mathbf{x}_2 + \mathbf{d}_1, \dot{\mathbf{x}}_2 = \mathbf{f}(\mathbf{x}_1, \mathbf{x}_2) + \mathbf{u} + \mathbf{d}_2, \mathbf{y} = \mathbf{x}_1$$

where $\mathbf{x}_1, \mathbf{x}_2 \in \mathbb{R}^m$ are the state vectors, $\mathbf{u} \in \mathbb{R}^m$ is the control input vector, $\mathbf{y} \in \mathbb{R}^m$ is the system output vector, $\mathbf{f}(\mathbf{x}_1, \mathbf{x}_2) \in \mathbb{R}^m$ is the state function vector, and $\mathbf{d}_1, \mathbf{d}_2 \in \mathbb{R}^m$ stand for the mismatched and matched disturbance vectors, respectively. Note that in the absence of mismatched disturbances, the MDOB-FT-SM-AC is reduced to the case of multivariable finite-time control under matched conditions.

Remark 6: In [15], the SMC with mismatched disturbances is considered for a scalar system. Meanwhile, in [16], the SMC with matched disturbances is examined for a multivariable system. Different from [15], [16], we here focus on the multivariable finite-time SMC with mismatched disturbances that is more proper for systems with strong couplings.

IV. SIMULATION VERIFICATION

For verification, the information of the inertia matrix $\mathbf{I}$ is borrowed from the Aerosonde UAV (see [1]). Also, for system (1), the initial conditions are zero. In light of [9], we set $\mathbf{d}_1 = [0.3\sin(t)\ \ 0.1\sin(2t)\ \ 0.2\sin(1.5t)]^\top$ and $\mathbf{d}_2 = [0.4\sin(2t)\ \ 0.2\sin(1.5t)\ \ 0.15\sin(t)]^\top$.[2] The desired command vector is $\mathbf{\Theta}_{\mathrm{ref}} = [-0.15 + 0.15\sin(1.5t)\ \ -0.05 +$

[2]It is straightforward to verify that $\mathbf{d}_1$ and $\mathbf{d}_2$ satisfy Assumption 1. Also, $\mathbf{d}_1$ and $\mathbf{d}_2$ are set as sinusoidal signals to show the capability of eliminating the effects of time-varying disturbances of the MDOB-FT-SM-AC.

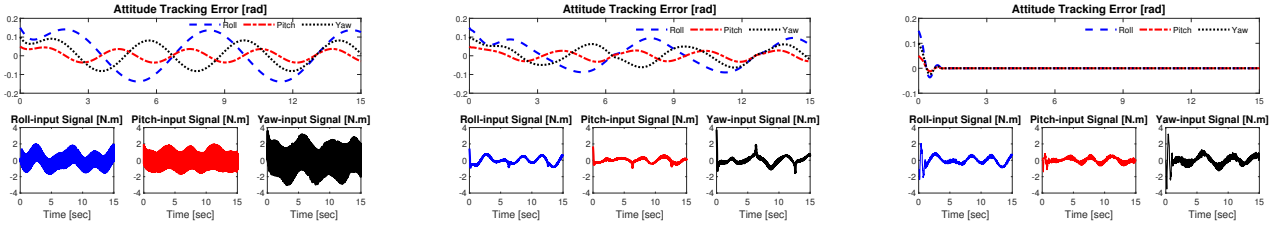

Fig. 1. Simulation results – From left to right: DOB-SM-AC, MSM-AC, MDOB-FT-SM-AC.

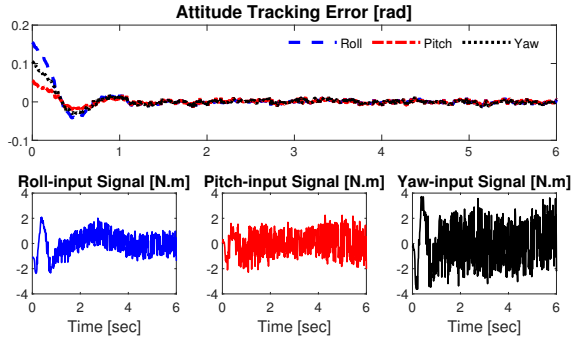

Fig. 2. Robustness verification – The proposed MDOB-FT-SM-AC.

$0.12\sin(t)\ -0.1+0.25\sin(0.8t)]^\top$. The controller parameters of the proposed MDOB-FT-SM-AC are selected as $\lambda_{01} = 2L_1^{1/3}, \lambda_{11} = 1.5\sqrt{2}L_1^{2/3}, \lambda_{21} = 1.1L_1, \lambda_{02} = 3\overline{L}_2^{1/2}, \lambda_{12} = 2.1\overline{L}_2, L_1 = 5.0, \overline{L}_2 = 5.0, k_1 = 5.0, k_2 = 3.5, r_1 = 3/7, r_2 = 3/5, \beta_1 = 5.0, \beta_2 = 1.0, \beta_3 = 8.0$, and $\beta_4 = 10.0$. Besides, for observers (7) and (8), the initial conditions of the terms $\mathbf{z}_{01}, \mathbf{z}_{11}, \mathbf{z}_{21}$, and $\mathbf{z}_{02}, \mathbf{z}_{12}$ are all set to zero.[3] For comparison purposes, the DOB sliding mode attitude control (DOB-SM-AC) in [5] and the multivariable sliding mode attitude control (MSM-AC) in [16] are implemented. For an adequate comparison, the control input torque for each channel is restricted in the range of $[-4.0; 4.0]$ (N.m).

As shown in Fig. 1, compared with the DOB-SM-AC and MSM-AC, the MDOB-FT-SM-AC exhibits the markedly better flight performance. In fact, the DOB-SM-AC and MSM-AC only drive $\mathbf{e}_1$ to some region around zero with considerable fluctuation due to the presence of mismatched disturbances. In addition, the DOB-SM-AC induces the serious chattering phenomenon. In contrast, the MDOB-FT-SM-AC enforces the attitude tracking error $\mathbf{e}_1$ to zero precisely and smoothly with significantly better control accuracy under the influences of mismatched disturbances. Besides, under the MDOB-FT-SM-AC, the chattering is noticeably alleviated.

We now verify the robustness of the MDOB-FT-SM-AC under measurement noises (see Remark 4). As regards of [1], the measurement noises, which adhere a normal distribution with a zero mean and variances of 0.004^2 and 0.002^2, are included in the Euler angle and angular rate signals. As shown in Fig. 2, the desirable flight performance and reasonable chattering alleviation are obtained even with noisy measurements.

[3]Note that the initial conditions of the terms $\mathbf{z}_{01}, \mathbf{z}_{11}, \mathbf{z}_{21}$, and $\mathbf{z}_{02}, \mathbf{z}_{12}$ should be selected appropriately depending on conditions of each flight scenario of the fixed-wing UAV such that the desirable control performance is achieved and the control input constraint is met.

V. CONCLUSIONS

This letter considered the MDOB-FT-SM-AC for disturbed fixed-wing UAVs. Possible future work is further improvement of the MDOB-FT-SM-AC under measurement noises.

REFERENCES

[1] R. W. Beard and T. W. McLain, *Small Unmanned Aircraft: Theory and Practice*. Princeton, NJ, USA: Princeton Univ. Press, 2012.

[2] T. Espinoza, A. Dzul, R. Lozano, and P. Parada, "Backstepping-sliding mode controllers applied to a fixed-wing UAV," *J. Intell. Robot. Syst.*, vol. 73, pp. 67–79, 2014.

[3] H. Castañeda, O. S. Salas-Peña, and J. de León-Morales, "Extended observer based on adaptive second order sliding mode control for a fixed wing UAV," *ISA Trans.*, vol. 66, pp. 226–232, 2017.

[4] C. Bao, Y. Guo, L. Luo, and G. Su, "Design of a fixed-wing UAV controller based on adaptive backstepping sliding mode control method," *IEEE Access*, vol. 9, pp. 157 825–157 841, 2021.

[5] L. Yu, G. He, S. Zhao, X. Wang, and L. Shen, "Immersion and invariance-based sliding mode attitude control of tilt tri-rotor UAV in helicopter mode," *Int. J. Control Autom. Syst.*, vol. 19, no. 2, pp. 722–735, 2021.

[6] Y. Song, Y. Tang, B. Ma, and B. Xu, "A singularity-free online neural network-based sliding mode control of the fixed-wing unmanned aerial vehicle optimal perching maneuver," *Optim. Control Appl. Methods*, vol. 44, no. 3, pp. 1425–1440, 2022.

[7] X.-H. Nian, W.-X. Zhou, S.-L. Li, and H.-Y. Wu, "2-D path following for fixed wing UAV using global fast terminal sliding mode control," *ISA Trans.*, vol. 136, pp. 162–172, 2023.

[8] L. Yu, G. He, X. Wang, and S. Zhao, "Robust fixed-time sliding mode attitude control of tilt trirotor UAV in helicopter mode," *IEEE Trans. Ind. Electron.*, vol. 69, no. 10, pp. 10 322–10 332, 2022.

[9] W.-H. Chen, J. Yang, L. Guo, and S. Li, "Disturbance-observer-based control and related methods – An overview," *IEEE Trans. Ind. Electron.*, vol. 63, no. 2, pp. 1083–1095, 2016.

[10] A. Levant, "Higher-order sliding modes, differentiation and output-feedback control," *Int. J. Control*, vol. 76, pp. 924–941, 2003.

[11] X. Shao, B. Tian, and W. Yang, "Fixed-time trajectory following for quadrotors via output feedback," *ISA Trans.*, vol. 110, pp. 213–224, 2021.

[12] I. Nagesh and C. Edwards, "A multivariable super-twisting sliding mode approach," *Automatica*, vol. 50, no. 3, pp. 984–988, 2014.

[13] H. K. Khalil, *Nonlinear Systems*. London, U.K.: Pearson, 2001.

[14] S. P. Bhat and D. S. Bernstein, "Geometric homogeneity with applications to finite-time stability," *Math. Control Signals Syst.*, vol. 17, pp. 101–127, 2005.

[15] J. Yang, S. Li, J. Su, and X. Yu, "Continuous nonsingular terminal sliding mode control for systems with mismatched disturbances," *Automatica*, vol. 49, no. 7, pp. 2287–2291, 2013.

[16] B. Tian, L. Liu, H. Lu, Z. Zuo, Q. Zong, and Y. Zhang, "Multivariable finite time attitude control for quadrotor UAV: Theory and experimentation," *IEEE Trans. Ind. Electron.*, vol. 65, pp. 2567–2577, 2018.